

# Irreversibility, Thermodynamic Uncertainty Relation, and Information Scrambling

Yoshihiko Hasegawa\*

Department of Information and Communication Engineering,  
Graduate School of Information Science and Technology,  
The University of Tokyo, Tokyo 113-8656, Japan

(Dated: March 1, 2022)

Entropy production characterizes irreversibility. This viewpoint induces us to regard thermodynamic uncertainty relation, stating that higher precision can be achieved at the cost of higher entropy production, as a relation between precision and the extent of irreversibility. In this Letter, we show that the precision of arbitrary Hermitian observables has a lower bound comprising the Loschmidt echo, which represents the irreversibility of quantum dynamics. Considering the continuous measurement in quantum Markov processes, the obtained relation can be viewed as a lower bound for the precision of counting observables, which is a quantum analog of thermodynamic uncertainty relation. Moreover, applying the obtained relation to the information scrambling, we obtain an upper bound for the out-of-time-order correlator.

*Introduction.*—Thermodynamic uncertainty relation (TUR) [1–17] (see [18] for a review) provides the universal relation between precision and thermodynamic cost. In the simplest form, it states  $\langle J \rangle^2 / \langle J \rangle^2 \geq 2 / \langle \sigma \rangle$ , where  $\langle J \rangle$  and  $\langle J \rangle$  are mean and standard deviation, respectively, of a current observable  $J$ , and  $\sigma$  is mean of the entropy production. TUR implies that higher precision can be achieved at a cost of higher entropy production. Entropy production quantifies the irreversibility of the system. Let  $\mathcal{P}_F(\Gamma)$  be probability to observe a trajectory  $\Gamma$  in the forward process, and  $\mathcal{P}_R(\bar{\Gamma})$  be that to observe a time-reversed trajectory  $\bar{\Gamma}$ . Then entropy production is defined by a log ratio between  $\mathcal{P}_F(\Gamma)$  and  $\mathcal{P}_R(\bar{\Gamma})$  [Fig. 1(a)]:

$$\sigma = \ln \frac{\mathcal{P}_F(\Gamma)}{\mathcal{P}_R(\bar{\Gamma})}. \quad (1)$$

This relation provides a viewpoint that TUR is a consequence of irreversibility, that is, the larger the extent of irreversibility, the higher the precision of thermodynamic machines becomes.

In Newtonian dynamics, despite microscopic reversibility, irreversibility emerges due to the chaotic nature of many-body systems. For chaotic many-body systems, even if we can consider the reversed dynamics by reverting the sign of momenta, an infinitely small perturbation applied to the state results in exponential divergence from the original reversed dynamics, implying that it is impossible to realize such reversed dynamics in reality. This viewpoint implies that the extent of irreversibility can be evaluated through the extent of chaos, which is often quantified by the Lyapunov exponent. The Loschmidt echo [19, 20] is an indicator for the effect of small perturbation applied to the Hamiltonian in quantum systems, which can be regarded as a quantum analog of the Lyapunov exponent. Consider an isolated quantum system. Given the initial pure state  $|\Psi(0)\rangle$ , Hamiltonian  $H$ , and its perturbed one  $H_*$ , the Loschmidt echo

is defined by

$$\eta \equiv |\langle \Psi(0) | e^{iH_*\tau} e^{-iH\tau} | \Psi(0) \rangle|^2. \quad (2)$$

Equation (2) evaluates the fidelity between two states,  $e^{-iH\tau} |\Psi(0)\rangle$  and  $e^{-iH_*\tau} |\Psi(0)\rangle$ , at time  $t = \tau$  [Fig. 1(b)]. These states are prepared by forward time evolution induced by  $H$  and  $H_*$ , respectively. Alternatively, Eq. (2) can be viewed as the fidelity between  $|\Psi(0)\rangle$  and  $e^{iH_*\tau} e^{-iH\tau} |\Psi(0)\rangle$  at  $t = 0$ , where the latter state is obtained by applying the forward time evolution by  $H$  and the subsequent reversed time evolution by  $H_*$  to  $|\Psi(0)\rangle$  [Fig. 1(c)]. The second interpretation provides a natural extension of the classical irreversibility. We show that the precision of Hermitian observables applied to the system has a lower bound comprising the Loschmidt echo. Specifically, when we consider the continuous measurement in quantum Markov processes, the precision of counting observables is bounded from below by the Loschmidt echo. This relation can be regarded as a quantum extension of the classical TURs, whose bound comprises the entropy production quantifying the irreversibility of classical Markov processes. Notably, the obtained quantum TUR holds for any continuous measurement, which has not been realized in the previous quantum TURs [21–30]. Moreover, we show that the main result can be applied to the information scrambling. We obtain an upper bound for the out-of-time-order correlation (OTOC), which quantifies the extent of quantum chaos and information spreading in quantum many-body systems.

*Results.*—We now relate the precision of Hermitian observables with the Loschmidt echo  $\eta$  defined in Eq. (2). Given the two Hamiltonians  $H$  and  $H_*$  in Eq. (2), we assume that  $|\Psi\rangle$  and  $|\Psi_*\rangle$  are time evolution induced by  $H$  and  $H_*$ , respectively, that is,  $|\Psi\rangle = e^{-iH\tau} |\Psi(0)\rangle$  and  $|\Psi_*\rangle = e^{-iH_*\tau} |\Psi(0)\rangle$  [Fig. 1(b)]. Let  $\mathcal{F}$  be a general Hermitian measurement operator on  $|\Psi\rangle$  and  $|\Psi_*\rangle$ .  $\mathcal{F}$  admits the eigendecomposition  $\mathcal{F} = \sum_z f(z) \Lambda(z)$ , where  $f(z)$  and  $\Lambda(z)$  are an eigenvalue and its corresponding

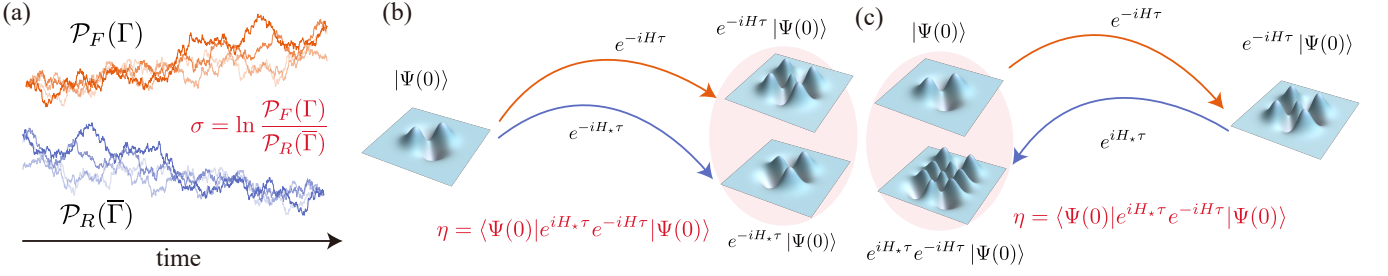


FIG. 1. Quantification of irreversibility. (a) Entropy production  $\sigma$  in classical Markov processes, which is defined by a log-ratio between  $\mathcal{P}_F(\Gamma)$ , probability to observe a trajectory  $\Gamma$  in the forward process, and  $\mathcal{P}_R(\bar{\Gamma})$ , that to observe a time-reversed trajectory  $\bar{\Gamma}$  in the reversed process. (b) Loschmidt echo  $\eta$  in quantum dynamics, which is the fidelity between two states,  $e^{-iH\tau}|\Psi(0)\rangle$  and  $e^{-iH_*\tau}|\Psi(0)\rangle$  at  $t = \tau$ . These states are obtained by forward time evolution induced by  $H$  and  $H_*$ , respectively. (c) Another viewpoint of Loschmidt echo  $\eta$ , which is the fidelity between two states,  $|\Psi(0)\rangle$  and  $e^{iH_*\tau}e^{-iH\tau}|\Psi(0)\rangle$ , at  $t = 0$ . The latter state is obtained by forward time evolution by  $H$  and the subsequent reversed time evolution by  $H_*$ .

projector, respectively. By using the projector  $\Lambda(z)$  in Eq. (11), the fidelity is bounded from above by

$$\begin{aligned} |\langle \Psi_* | \Psi \rangle| &\leq \sum_z |\langle \Psi_* | \Lambda(z) | \Psi \rangle| \\ &\leq \sum_z \sqrt{\langle \Psi_* | \Lambda(z) | \Psi_* \rangle} \sqrt{\langle \Psi | \Lambda(z) | \Psi \rangle} \\ &= 1 - \mathcal{H}^2(P, P_*). \end{aligned} \quad (3)$$

where  $P(z) \equiv \langle \Psi | \Lambda(z) | \Psi \rangle$ ,  $P_*(z) \equiv \langle \Psi_* | \Lambda(z) | \Psi_* \rangle$ , and  $\mathcal{H}^2(\bullet, \bullet)$  is the Hellinger distance. The Hellinger distance is defined by

$$\mathcal{H}^2(P, P_*) = \frac{1}{2} \sum_z \left( \sqrt{P(z)} - \sqrt{P_*(z)} \right)^2, \quad (4)$$

where  $0 \leq \mathcal{H}^2(P, P_*) \leq 1$ . Therefore, the Hellinger distance quantifies the similarity between the two distributions. The Hellinger distance has a lower bound given mean and variance [31–33]. In particular, we use a tighter lower bound recently derived in Ref. [33]:

$$\mathcal{H}^2(P, Q) \geq 1 - \left[ \left( \frac{\langle f \rangle_P - \langle f \rangle_Q}{\sqrt{\langle f^2 \rangle_P + \langle f^2 \rangle_Q}} \right)^2 + 1 \right]^{-\frac{1}{2}}, \quad (5)$$

where  $\langle f \rangle_P \equiv \sum_z f(z)P(z)$  and  $\sqrt{\langle f^2 \rangle_P} \equiv \sqrt{\langle f^2 \rangle_P - \langle f \rangle_P^2}$  stand for mean standard deviation, respectively. Substituting Eq. (5) to Eq. (3), we obtain

$$\left( \frac{\sqrt{\langle \mathcal{F} \rangle + \langle \mathcal{F} \rangle_*}}{\sqrt{\langle \mathcal{F} \rangle - \langle \mathcal{F} \rangle_*}} \right)^2 \geq \frac{1}{\eta^{-1} - 1}. \quad (6)$$

where  $\langle \mathcal{F} \rangle \equiv \langle \Psi | \mathcal{F} | \Psi \rangle$  and  $\sqrt{\langle \mathcal{F}^2 \rangle} \equiv \sqrt{\langle \mathcal{F}^2 \rangle - \langle \mathcal{F} \rangle^2}$  (quantities with  $*$  should be evaluated for  $|\Psi_*\rangle$  instead of  $|\Psi\rangle$ ). Equation (6) is the main result of this Letter. Equation (6) shows that the precision is bounded from below by the Loschmidt echo  $\eta$ . When the system becomes more irreversible (that is, smaller  $\eta$ ), the precision can

be improved. Note that if we employ a lower bound of the Hellinger distance in Refs. [31, 32], we obtain a different bound.

*Thermodynamic uncertainty relation.*—TURs in classical Markov processes consider an observable which is a function of a stochastic trajectory generated by a classical Markov process. Using Eq. (6), we can obtain a TUR for quantum Markov processes. We consider a quantum Markov process described by a Lindblad equation [34, 35]. Let  $\rho_S(t)$  be a density operator at time  $t$ . The time evolution of  $\rho_S(t)$  is governed by

$$\dot{\rho}_S = \mathcal{L}\rho_S \equiv -i[H_S, \rho_S] + \sum_{m=1}^M \mathcal{D}(\rho_S, L_m), \quad (7)$$

where  $\mathcal{L}$  is a Lindblad super-operator,  $H_S$  is a Hamiltonian,  $\mathcal{D}(\rho_S, L) \equiv [L\rho_S L^\dagger - \{L^\dagger L, \rho_S\}]/2$  is a dissipator, and  $L_m$  ( $1 \leq m \leq M$  with  $M$  being the number of jump operators) is an  $m$ th jump operator ( $[\bullet, \bullet]$  and  $\{\bullet, \bullet\}$  denote the commutator and anticommutator, respectively). Note that  $H_S$  is different from the total Hamiltonian  $H$ , which induces unitary time evolution on the isolated system. For a sufficiently small time interval  $\Delta t$ , the Lindblad equation of Eq. (7) admits the Kraus representation  $\rho_S(t + \Delta t) = \sum_{m=0}^M V_m \rho_S(t) V_m^\dagger$ , where

$$V_0 \equiv \mathbb{I}_S - i\Delta t H_S - \frac{1}{2}\Delta t \sum_{m=1}^M L_m^\dagger L_m, \quad (8)$$

$$V_m \equiv \sqrt{\Delta t} L_m \quad (1 \leq m \leq M), \quad (9)$$

where  $\mathbb{I}_S$  denote the identity operator in  $S$  (the other identity operators are defined in the same way).  $V_0$  corresponds to no jump and  $V_m$  ( $1 \leq m \leq M$ ) to  $m$ th jump within the interval  $[t, t + \Delta t]$ .  $V_m$  ( $0 \leq m \leq M$ ) satisfies a completeness relation  $\sum_{m=0}^M V_m^\dagger V_m = \mathbb{I}_S$ . As discussed later,  $V_m$  defined in Eqs. (8) and (9) are not only operators that are consistent with Eq. (7). There are infinitely many operators that can induce the same time evolution.

Using the input-output formalism [36–39], we describe the time evolution generated by the Kraus operators (8) and (9) as interactions between the principal system  $S$  and the environment  $E$  [Fig. 2(a)]. Let  $t = 0$  and  $t = \tau$  be the initial and the final time, respectively, of the time evolution. We discretize the time interval  $[0, \tau]$  by dividing it into  $N$  intervals, where  $N$  is a sufficiently large number, and we define  $\Delta t \equiv \tau/N$  and  $t_k \equiv \Delta t k$  ( $t_0 = 0$  and  $t_N = \tau$ ). Here, the orthonormal basis of  $E$  is assumed to be  $|m_{N-1}, \dots, m_1, m_0\rangle$  ( $m_k \in \{0, 1, \dots, M-1, M\}$ ), where a subspace  $|m_k\rangle$  interacts with  $S$  via a unitary operator  $U_{t_k}$  during an interval  $[t_k, t_{k+1}]$  [Fig. 2(a)]. When the initial states of  $S$  and  $E$  are  $|\psi_S\rangle$  and  $|0_{N-1}, \dots, 0_1, 0_0\rangle$ , respectively, the composite state at  $t = \tau$  is

$$\begin{aligned} |\Psi(\tau)\rangle &= U_{t_{N-1}} \cdots U_{t_0} |\psi_S\rangle \otimes |0_{N-1}, \dots, 0_0\rangle \\ &= \sum_{\mathbf{m}} V_{m_{N-1}} \cdots V_{m_0} |\psi_S\rangle \otimes |m_{N-1}, \dots, m_0\rangle, \end{aligned} \quad (10)$$

where  $V_{m_k} = \langle m_k | U_{t_k} | 0_k \rangle$  is an action on  $S$ , which is associated with the transition from  $|0_k\rangle$  to  $|m_k\rangle$  in  $E$ . If we calculate  $\text{Tr}_E[|\Psi(\tau)\rangle \langle \Psi(\tau)|]$  for  $\Delta t \rightarrow 0$ , we recover the original Lindblad equation of Eq. (7).

Continuous measurement [40, 41] of the principal system via the environment at each time interval corresponds to measuring the environment at the final time [Fig. 2(a)]. When we measure the environment at  $t = \tau$  with projectors  $\Pi(\mathbf{m}) = |\mathbf{m}\rangle \langle \mathbf{m}|$  with  $\mathbf{m} \equiv [m_{N-1}, \dots, m_1, m_0]$ , we obtain a realization of  $\mathbf{m}$  and the principal system becomes  $V_{m_{N-1}} \cdots V_{m_0} |\psi_S\rangle$  (note that this state is unnormalized). Therefore,  $\mathbf{m}$  constitutes a measurement record of the continuous measurement. Because the evolution of  $V_{m_{N-1}} \cdots V_{m_0} |\psi_S\rangle$  is stochastic depending on the measurement record, it is referred to as a quantum trajectory which can be described by the stochastic Schrödinger equation [42]. In classical TURs, we are interested in a counting observable that counts and weights transitions in the stochastic trajectory. The counting observable in the classical stochastic thermodynamics is  $\sum_{j \neq i} C_{ji} \mathcal{N}_{ji}$ , where  $\mathcal{N}_{ji}$  is the number of transitions from  $i$ th to  $j$ th state during the time interval, and  $C_{ji} \in \mathbb{R}$  is its weight. The *current* observable assumes anti-symmetry  $C_{ji} = -C_{ij}$ , which is a special case of the counting observable. Similarly, in a quantum Markov process, we wish to count the number of jumps in a quantum trajectory. Let us consider an Hermitian measurement operator  $\mathcal{G}$  on  $E$ , which admits the following eigendecomposition:

$$\mathcal{G} = \sum_{\mathbf{m}} g(\mathbf{m}) \Pi(\mathbf{m}). \quad (11)$$

We assume that  $g(\mathbf{m})$  in Eq. (11) counts and weights jumps in  $\mathbf{m}$ , which defines a counting observable in quantum Markov processes. Specifically, we may use  $g(\mathbf{m}) = \sum_{k=0}^{N-1} C_{m_k}$ , where  $C \equiv [0, a_1, \dots, a_M]$  ( $a_i \in \mathbb{R}$ ) is

a projection vector specifying the weight of each jump. For instance, when  $M = 1$  (there is a single jump operator), an example of the measurement record is something like  $\mathbf{m} = [0, 0, 1, 0, \dots, 0, 1, 0, 0]$  where 1s denote the detection of jumps. When  $C = [0, 1]$ ,  $g(\mathbf{m})$  simply counts the number of jumps in  $\mathbf{m}$ . Then  $\langle \Psi(\tau) | \mathbb{I}_S \otimes \mathcal{G} | \Psi(\tau) \rangle$  and  $\langle \Psi(\tau) | \mathbb{I}_S \otimes \mathcal{G}^2 | \Psi(\tau) \rangle - \langle \Psi(\tau) | \mathbb{I}_S \otimes \mathcal{G} | \Psi(\tau) \rangle^2$  yield mean and variance of the number of jumps within the interval  $[0, \tau]$ .

The Loschmidt echo concerns the fidelity between the original  $|\Psi\rangle$  and the perturbed state  $|\Psi_\star\rangle$  [Eq. (2)]. Let  $H_{\star,S}$  and  $L_{\star,m}$  ( $1 \leq m \leq M$ ) be the perturbed Hamiltonian and the jump operator in Eqs. (8) and (9). Then  $V_{\star,m}$ , the Kraus operators of the perturbed dynamics, can be defined through Eqs. (8) and (9), where  $H_S$  and  $L_m$  should be replaced with  $H_{\star,S}$  and  $L_{\star,m}$ , respectively. Similar to Eq. (10), the composite state of the perturbed dynamics at  $t = \tau$  is

$$|\Psi_\star(\tau)\rangle = \sum_{\mathbf{m}} V_{\star,m_{N-1}} \cdots V_{\star,m_0} |\psi_S\rangle \otimes |m_{N-1}, \dots, m_0\rangle. \quad (12)$$

Calculation of the Loschmidt echo  $|\langle \Psi_\star | \Psi \rangle|^2$  for Eqs. (10) and (12) appears to be a formidable task because the composite state  $|\Psi(\tau)\rangle$  or  $|\Psi_\star(\tau)\rangle$ , comprising the principal system and the environment, is not accessible in general. However, for the continuous measurement, the Loschmidt echo can be computed explicitly after Refs. [37, 43]. Notice that  $\langle \Psi_\star | \Psi \rangle = \text{Tr}_{SE} [|\Psi\rangle \langle \Psi_\star|] = \text{Tr}_S [\phi]$  where  $\phi(t) \equiv \text{Tr}_E [|\Psi(t)\rangle \langle \Psi_\star(t)|]$ . Therefore, by using Eqs. (10) and (12),  $\phi$  satisfies a two-sided Lindblad equation [37, 43]:  $\dot{\phi} = \mathcal{K}\phi \equiv -iH_S\phi + i\phi H_{S,\star} + \sum_m L_m \phi L_{\star,m}^\dagger - \frac{1}{2} \sum_m [L_m^\dagger L_m \phi + \phi L_{\star,m}^\dagger L_{\star,m}]$ , where  $\mathcal{K}$  is a super-operator. Note that  $\phi$  does not preserve the trace, that is,  $\text{Tr}_S[\phi(t)] \neq 1$  in general. By solving the two-sided Lindblad equation, the solution is  $\phi(\tau) = e^{\mathcal{K}\tau} \rho_S(0)$  where  $\rho_S(0) = |\psi_S\rangle \langle \psi_S|$  is the initial density operator of the Lindblad dynamics [44]. The Loschmidt echo  $\eta$  is expressed by  $\eta = |\text{Tr}_S [e^{\mathcal{K}\tau} \rho_S(0)]|^2$ . Importantly,  $\eta$  can be specified by quantities of  $S$  alone ( $H_S$ ,  $L_m$ ,  $H_{\star,S}$ , and  $L_{\star,m}$ ). We do not require information about  $E$ , which is not accessible in general. Calculations above assumed an initially pure state; however, generalization to an initially mixed state case is straightforward [42]. By taking  $\mathcal{F} = \mathbb{I}_S \otimes \mathcal{G}$  in Eq. (6), where  $\mathcal{G}$  is the counting observable defined in Eq. (11), we obtain

$$\left( \frac{[\mathcal{G}] + [\mathcal{G}]_\star}{\langle \mathcal{G} \rangle - \langle \mathcal{G} \rangle_\star} \right)^2 \geq \frac{1}{|\text{Tr}_S [e^{\mathcal{K}\tau} \rho_S(0)]|^{-2} - 1}. \quad (13)$$

Equation (13) shows that the precision of counting observables is improved when the extent of irreversibility becomes higher, which qualitatively agrees with classical TURs [1, 2]. Classical TURs have the lower bound comprising the entropy production that characterizes the irreversibility of classical Markov processes. The Kraus

operator  $V_m$  in Eqs. (8) and (9) are not unique and depend on the continuous measurement. We can show that Eq. (13) holds for any continuous measurement [42].

We consider a specific case that the perturbed dynamics is empty in Eq. (13), that is,  $H_{S,*} = 0$  and  $L_{*,m} = 0$  for all  $m$ . In this case, the composite state of the perturbed dynamics at  $t = \tau$  is  $|\Psi_*(\tau)\rangle = |\psi_S\rangle \otimes |0_{N-1}, \dots, 0_0\rangle$ , which is unchanged from the initial state. Because  $\mathcal{G}$  counts the number of jumps in the measurement record  $\mathbf{m}$ , it should vanish at the initial state because there is no jump at  $t = 0$ . Therefore  $\langle \mathcal{G} \rangle_* = 0$  and  $\|\mathcal{G}\|_* = 0$  for the empty dynamics. Equation (6) becomes

$$\frac{\|\mathcal{G}\|^2}{\langle \mathcal{G} \rangle^2} \geq \frac{1}{\left| \text{Tr}_S \left[ e^{(-iH_S - \frac{1}{2} \sum_m L_m^\dagger L_m) \tau} \rho_S(0) \right] \right|^{-2} - 1}. \quad (14)$$

The bound of Eq. (14) is similar to that obtained in Ref. [29]. Note that there is no definite magnitude relation between Eq. (14) and Ref. [29]. In short time limit  $\tau \rightarrow 0$ , we obtain  $\|\mathcal{G}\|^2 / \langle \mathcal{G} \rangle^2 \geq 1 / [\text{Tr}_S[\sum_m L_m^\dagger L_m \rho_S(0) \tau]]$ , where the denominator corresponds to the dynamical activity [45] in classical Markov processes. Although Eq. (13) does not depend on the continuous measurement, Eq. (14) only holds for the continuous measurement corresponding to Eqs. (8) and (9).

We perform a numerical simulation for the continuous measurement. We consider photon counting in a two-level atom driven by a laser field. Let  $|\epsilon_g\rangle$  and  $|\epsilon_e\rangle$  denote ground and excite states, respectively. The Lindblad equation of the system is  $H_S = \Delta |\epsilon_e\rangle \langle \epsilon_e| + (\Omega/2)(|\epsilon_e\rangle \langle \epsilon_g| + |\epsilon_g\rangle \langle \epsilon_e|)$  and  $L = \sqrt{\kappa} |\epsilon_g\rangle \langle \epsilon_e|$ , where  $\Delta$ ,  $\Omega$ , and  $\kappa$  are model parameters. Equation (6) concerns two dynamics, that is, the original and its perturbed dynamics. For each dynamics, we randomly select the model parameters  $\Delta$ ,  $\Omega$ , and  $\kappa$  (that is, 6 model parameters in total). The time duration  $\tau$  is randomly sampled (see the caption of Fig. 2(a) for the parameter ranges), and the initial density operator  $\rho_S$  is determined randomly as well. For the selected parameters and the density operator, we generate many quantum trajectories and calculate  $(\|\mathcal{G}\| + \|\mathcal{G}\|_*)^2 / (\langle \mathcal{G} \rangle - \langle \mathcal{G} \rangle_*)^2$ . In Fig. 2(a), we plot  $(\|\mathcal{G}\| + \|\mathcal{G}\|_*)^2 / (\langle \mathcal{G} \rangle - \langle \mathcal{G} \rangle_*)^2$  as a function of  $(\eta^{-1} - 1)^{-1}$  with  $\eta = |\text{Tr}_S[e^{K\tau} \rho_S(0)]|^2$  (which is the right hand side of Eq. (6)) by circles, where the dashed line denotes the lower bound. All circles are located above the line, verifying Eq. (6) for the driven two-level atom system. As denoted above, Eq. (6) should hold for any continuous measurement (that is, any unraveling). Therefore, we also perform a numerical simulation for different continuous measurements and verify the bound (see Ref. [42] for details).

*Information scrambling.*—We next apply Eq. (6) to the information scrambling. In the information scrambling, OTOC [48], which was originally introduced by Ref. [49],

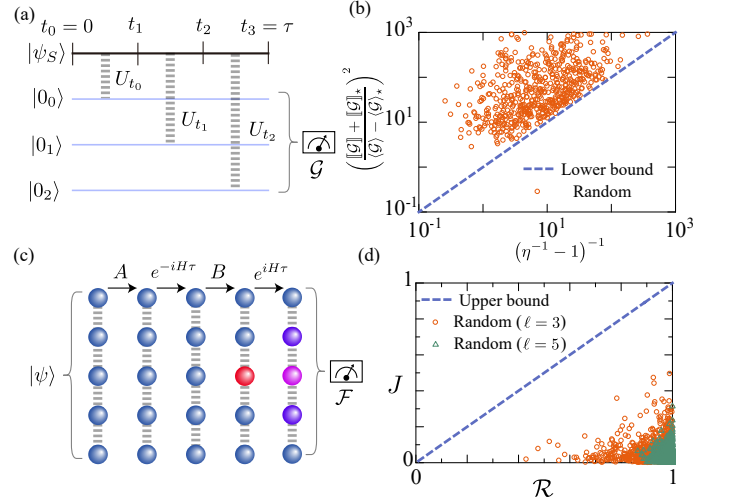


FIG. 2. Applications of the main result [Eq. (6)]. (a) Illustration of continuous measurement model for  $N = 3$  case. The initial state of  $S$  and  $E$  are  $|\psi_S\rangle$  and  $|0_2, 0_1, 0_0\rangle$ , respectively. The environment subspace  $|m_k\rangle$  interacts with  $S$  via a unitary operator  $U_{t_k}$  during an interval  $[t_k, t_{k+1}]$ . Finally at  $t = \tau$ ,  $E$  is measured by  $\mathcal{G}$ . (b) Precision  $(\|\mathcal{G}\| + \|\mathcal{G}\|_*)^2 / (\langle \mathcal{G} \rangle - \langle \mathcal{G} \rangle_*)^2$  as a function of  $(\eta^{-1} - 1)^{-1}$  for random realizations, where  $\eta$  is the Loschmidt echo  $\eta = |\text{Tr}_S[e^{K\tau} \rho_S(0)]|^2$ . The dashed line denote the lower bound of the precision shown in Eq. (13). The parameter ranges are  $\Delta \in [0.1, 3.0]$ ,  $\Omega \in [0.1, 3.0]$ , and  $\kappa \in [0.1, 3.0]$  for each dynamics, and  $\tau \in [0.1, 1.0]$ . (c) Illustration of information scrambling in Ising spin chain ( $\ell = 5$ ).  $|\Psi\rangle$  is prepared by applying in order of  $A$ ,  $e^{-iH\tau}$ ,  $B$ , and  $e^{iH\tau}$  to  $|\psi\rangle$ . Finally, the system is measured by  $\mathcal{F}$ . (d) Loschmidt echo  $\eta$  as a function  $\mathcal{R}$  defined in Eq. (18) for random realization of Ising spin chain with the length  $\ell = 3$  (circles) and  $\ell = 5$  (triangles). The dashed line denote the upper bound of  $\eta$ . The other parameters are  $g = (\sqrt{5} + 5)/8$  and  $h = (\sqrt{5} + 1)/4$  which are identical to Refs. [46, 47].

plays a fundamental role. OTOC is regarded as an important indicator for the extent of quantum chaos and information spreading in quantum many-body systems. Given a pure state  $|\psi\rangle$ , OTOC  $J(\tau)$  is defined by

$$J(\tau) \equiv |\langle \psi | B^\dagger(\tau) A^\dagger B(\tau) A | \psi \rangle|^2, \quad (15)$$

where  $A, B$  are arbitrary Hermitian or unitary operators. Here  $B(\tau) = e^{iH\tau} B e^{-iH\tau}$  is a Heisenberg interpretation of the operator  $B$ , where  $H$  is a total Hamiltonian which induces the unitary time evolution  $e^{-iH\tau}$ . Let us obtain the bound for OTOC via Eq. (6). Specifically, we assume that  $A$  and  $B$  are both unitary operators. In Eq. (6), we consider the following states:

$$|\Psi\rangle = e^{iH\tau} B e^{-iH\tau} A |\psi\rangle, \quad (16)$$

$$|\Psi_*\rangle = A e^{iH\tau} B e^{-iH\tau} |\psi\rangle. \quad (17)$$

$|\Psi\rangle$  in Eq. (16) is obtained by successive application of the unitary  $A$ ,  $e^{-iH\tau}$  (the forward time evolution by  $H$ ), the unitary  $B$ , and  $e^{iH\tau}$  (the forward time evolution by  $-H$ ). On the other hand, for  $|\Psi_*\rangle$ , we apply unitary



operators in order of  $e^{-iH\tau}$ ,  $B$ ,  $e^{iH\tau}$ , and  $A$ . Because the OTOC is  $|\langle\Psi_\star|\Psi\rangle|^2$ , substituting Eqs. (16) and (17) to Eq. (6), we can obtain an upper bound for OTOC,  $J(\tau) \leq \mathcal{R}$  where

$$\mathcal{R} \equiv \left[ 1 + \left( \frac{\langle \mathcal{F} \rangle - \langle \mathcal{F} \rangle_\star}{\|\mathcal{F}\| + \|\mathcal{F}\|_\star} \right)^2 \right]^{-1}. \quad (18)$$

Here  $\mathcal{F}$  is any measurement operator on  $|\Psi\rangle$  and  $|\Psi_\star\rangle$  in Eqs. (16) and (17). Equation (18) implies that mean and variance of  $\mathcal{F}$  provides an upper bound on the OTOC.

We perform a numerical simulation to verify Eq. (18). We consider an Ising spin chain model employed in Refs. [46, 47], where the spin is subject to both transverse and longitudinal fields. Let  $\ell$  be the length of the chain, and  $\sigma_x^i$  and  $\sigma_z^i$  be Pauli matrices of the spin at site  $i$ . The Hamiltonian of the system is  $H = H_0 + H_1$  with  $H_0 \equiv g \sum_{i=1}^{\ell} \sigma_x^i$  and  $H_1 \equiv J \sum_{i=1}^{\ell-1} \sigma_z^i \sigma_z^{i+1} + h \sum_{i=2}^{\ell-1} \sigma_z^i + (h - J)(\sigma_z^1 + \sigma_z^\ell)$ , where  $h$  is longitudinal field strength,  $J$  is the interaction strength, and  $g$  is transverse field strength. Following Ref. [47], for the operators  $A$  and  $B$  in Eq. (15), we select  $A = e^{iH_0}$  and  $B = e^{-i\theta\sigma_x^{i_c}}$  with  $\theta = \pi/2$  and  $i_c \equiv (L+1)/2$ . In this setting, when  $\ell$  is odd,  $B$  corresponds to the perturbing the center of the spin chain. The procedure for obtaining  $|\Psi\rangle$  in Eq. (16) is depicted in Fig. 2(c) for  $\ell = 5$ . We set the initial pure state  $|\psi\rangle = |b_1\rangle \otimes \cdots \otimes |b_\ell\rangle$ , where each  $|b_i\rangle$  is selected randomly from the Bloch sphere. We randomly generate Hermitian operator  $\mathcal{F}$ , and calculate the right hand side of Eq. (18) for each random case [the parameter settings are shown in the caption of Fig. 2(d)]. In Fig. 2(d), we plot the OTOC  $J$  as a function of  $\mathcal{R}$  for  $\ell = 3$  (circles) and  $\ell = 5$  (triangles), where the dashed line denote the upper bound of Eq. (18). We see that all the realizations are located below the dashed line, verifying Eq. (18) numerically. For  $\ell = 5$ , the bound becomes looser, indicating that Eq. (18) is tighter for smaller systems. Although Eq. (18) confers a rather rough upper bound for the OTOC, this way of narrowing down the range of OTOC has a practical advantage because we only have to simply observe  $|\Psi\rangle$  and  $|\Psi_\star\rangle$ .

**Conclusion.**—In this letter, we have found a relation between the Loschmidt echo and the precision. When considering the continuous measurement in quantum Markov processes, the obtained bound can be regarded as a quantum generalization of TURs. Moreover, our bound can be applied to obtain the bound for the OTOC, which is an important indicator in information scrambling. It is expected that we can obtain other thermodynamic relations through the main result.

This work was supported by the Ministry of Education, Culture, Sports, Science and Technology (MEXT) KAKENHI Grant No. JP19K12153.

\* [hasegawa@biom.t.u-tokyo.ac.jp](mailto:hasegawa@biom.t.u-tokyo.ac.jp)

- [1] A. C. Barato and U. Seifert, Thermodynamic uncertainty relation for biomolecular processes, *Phys. Rev. Lett.* **114**, 158101 (2015).
- [2] T. R. Gingrich, J. M. Horowitz, N. Perunov, and J. L. England, Dissipation bounds all steady-state current fluctuations, *Phys. Rev. Lett.* **116**, 120601 (2016).
- [3] P. Pietzonka, A. C. Barato, and U. Seifert, Universal bounds on current fluctuations, *Phys. Rev. E* **93**, 052145 (2016).
- [4] J. M. Horowitz and T. R. Gingrich, Proof of the finite-time thermodynamic uncertainty relation for steady-state currents, *Phys. Rev. E* **96**, 020103 (2017).
- [5] S. Pigolotti, I. Neri, E. Roldán, and F. Jülicher, Generic properties of stochastic entropy production, *Phys. Rev. Lett.* **119**, 140604 (2017).
- [6] J. P. Garrahan, Simple bounds on fluctuations and uncertainty relations for first-passage times of counting observables, *Phys. Rev. E* **95**, 032134 (2017).
- [7] A. Dechant and S.-i. Sasa, Current fluctuations and transport efficiency for general Langevin systems, *J. Stat. Mech: Theory Exp.* **2018**, 063209 (2018).
- [8] A. C. Barato, R. Chetrite, A. Faggionato, and D. Gabrielli, Bounds on current fluctuations in periodically driven systems, *New J. Phys.* **20** (2018).
- [9] I. D. Terlizzi and M. Baiesi, Kinetic uncertainty relation, *J. Phys. A: Math. Theor.* **52**, 02LT03 (2019).
- [10] Y. Hasegawa and T. Van Vu, Uncertainty relations in stochastic processes: An information inequality approach, *Phys. Rev. E* **99**, 062126 (2019).
- [11] Y. Hasegawa and T. Van Vu, Fluctuation theorem uncertainty relation, *Phys. Rev. Lett.* **123**, 110602 (2019).
- [12] T. Van Vu and Y. Hasegawa, Uncertainty relations for underdamped Langevin dynamics, *Phys. Rev. E* **100**, 032130 (2019).
- [13] T. Van Vu and Y. Hasegawa, Thermodynamic uncertainty relations under arbitrary control protocols, *Phys. Rev. Research* **2**, 013060 (2020).
- [14] A. Dechant and S.-i. Sasa, Fluctuation–response inequality out of equilibrium, *Proc. Natl. Acad. Sci. U.S.A.* **117**, 6430 (2020).
- [15] V. T. Vo, T. Van Vu, and Y. Hasegawa, Unified approach to classical speed limit and thermodynamic uncertainty relation, *Phys. Rev. E* **102**, 062132 (2020).
- [16] T. Koyuk and U. Seifert, Thermodynamic uncertainty relation for time-dependent driving, *Phys. Rev. Lett.* **125**, 260604 (2020).
- [17] A. Dechant and S. ichi Sasa, Continuous time-reversal and equality in the thermodynamic uncertainty relation, *arXiv:2010.14769* (2020).
- [18] J. M. Horowitz and T. R. Gingrich, Thermodynamic uncertainty relations constrain non-equilibrium fluctuations, *Nat. Phys.* (2019).
- [19] A. Peres, Stability of quantum motion in chaotic and regular systems, *Phys. Rev. A* **30**, 1610 (1984).
- [20] A. Goussev, R. A. Jalabert, H. M. Pastawski, and D. Wisniacki, Loschmidt echo, *arXiv:1206.6348* (2012).
- [21] P. Erker, M. T. Mitchison, R. Silva, M. P. Woods, N. Brunner, and M. Huber, Autonomous quantum clocks: Does thermodynamics limit our ability to measure time?, *Phys. Rev. X* **7**, 031022 (2017).

- [22] K. Brandner, T. Hanazato, and K. Saito, Thermodynamic bounds on precision in ballistic multiterminal transport, *Phys. Rev. Lett.* **120**, 090601 (2018).
- [23] F. Carollo, R. L. Jack, and J. P. Garrahan, Unraveling the large deviation statistics of Markovian open quantum systems, *Phys. Rev. Lett.* **122**, 130605 (2019).
- [24] J. Liu and D. Segal, Thermodynamic uncertainty relation in quantum thermoelectric junctions, *Phys. Rev. E* **99**, 062141 (2019).
- [25] G. Guarnieri, G. T. Landi, S. R. Clark, and J. Goold, Thermodynamics of precision in quantum nonequilibrium steady states, *Phys. Rev. Research* **1**, 033021 (2019).
- [26] S. Saryal, H. M. Friedman, D. Segal, and B. K. Agarwalla, Thermodynamic uncertainty relation in thermal transport, *Phys. Rev. E* **100**, 042101 (2019).
- [27] Y. Hasegawa, Quantum thermodynamic uncertainty relation for continuous measurement, *Phys. Rev. Lett.* **125**, 050601 (2020).
- [28] H. M. Friedman, B. K. Agarwalla, O. Shein-Lumbroso, O. Tal, and D. Segal, Thermodynamic uncertainty relation in atomic-scale quantum conductors, *Phys. Rev. B* **101**, 195423 (2020).
- [29] Y. Hasegawa, Thermodynamic uncertainty relation for general open quantum systems, *Phys. Rev. Lett.* **126**, 010602 (2021).
- [30] M. F. Sacchi, Thermodynamic uncertainty relations for bosonic Otto engines, *Phys. Rev. E* **103**, 012111 (2021).
- [31] M. Dashti and A. M. Stuart, The Bayesian approach to inverse problems, in *Handbook of Uncertainty Quantification*, edited by R. Ghanem, D. Higdon, and H. Owhadi (2017) pp. 311–428.
- [32] M. A. Katsoulakis, L. Rey-Bellet, and J. Wang, Scalable information inequalities for uncertainty quantification, *J. Comput. Phys.* **336**, 513 (2017).
- [33] T. Nishiyama, A tight lower bound for the Hellinger distance with given means and variances, *arXiv:2010.13548* (2020).
- [34] G. Lindblad, On the generators of quantum dynamical semigroups, *Commun. Math. Phys.* **48**, 119 (1976).
- [35] H.-P. Breuer and F. Petruccione, *The theory of open quantum systems* (Oxford university press, 2002).
- [36] M. Guță, Fisher information and asymptotic normality in system identification for quantum Markov chains, *Phys. Rev. A* **83**, 062324 (2011).
- [37] S. Gammelmark and K. Mølmer, Fisher information and the quantum Cramér-Rao sensitivity limit of continuous measurements, *Phys. Rev. Lett.* **112**, 170401 (2014).
- [38] K. Macieszczak, M. Guță, I. Lesanovsky, and J. P. Garrahan, Dynamical phase transitions as a resource for quantum enhanced metrology, *Phys. Rev. A* **93**, 022103 (2016).
- [39] J. A. Gross, C. M. Caves, G. J. Milburn, and J. Combes, Qubit models of weak continuous measurements: Markovian conditional and open-system dynamics, *Quantum Sci. Technol.* **3**, 024005 (2018).
- [40] H. M. Wiseman, Quantum trajectories and quantum measurement theory, *J. Eur. Opt. Soc. Part B* **8**, 205 (1996).
- [41] C. Elouard and M. H. Mohammady, Work, heat and entropy production along quantum trajectories, in *Thermodynamics in the Quantum Regime: Fundamental Aspects and New Directions*, edited by F. Binder, L. A. Correa, C. Gogolin, J. Anders, and G. Adesso (Springer International Publishing, Cham, 2018) pp. 363–393.
- [42] See Supplemental Material.
- [43] K. Mølmer, Hypothesis testing with open quantum systems, *Phys. Rev. Lett.* **114**, 040401 (2015).
- [44] Since  $\mathcal{K}$  is a super-operator, evaluation of  $e^{\mathcal{K}\tau}$  requires calculation in the Liouville space.
- [45] C. Maes, Frenesy: Time-symmetric dynamical activity in nonequilibria, *Phys. Rep.* **850**, 1 (2020).
- [46] H. Kim and D. A. Huse, Ballistic spreading of entanglement in a diffusive nonintegrable system, *Phys. Rev. Lett.* **111**, 127205 (2013).
- [47] M. Campisi and J. Goold, Thermodynamics of quantum information scrambling, *Phys. Rev. E* **95**, 062127 (2017).
- [48] B. Swingle, Unscrambling the physics of out-of-time-order correlators, *Nat. Phys.* **14**, 988 (2018).
- [49] A. Larkin and Y. N. Ovchinnikov, Quasiclassical method in the theory of superconductivity, *Sov. Phys. JETP* **28**, 1200 (1969).

# Supplementary Material for “Irreversibility, Thermodynamic Uncertainty Relation, and Information Scrambling”

Yoshihiko Hasegawa\*

*Department of Information and Communication Engineering,  
Graduate School of Information Science and Technology,  
The University of Tokyo, Tokyo 113-8656, Japan*

This supplementary material describes the calculations introduced in the main text. Equation and figure numbers are prefixed with S (e.g., Eq. (S1) or Fig. S1). Numbers without this prefix (e.g., Eq. (1) or Fig. 1) refer to items in the main text.

## S1. THERMODYNAMIC UNCERTAINTY RELATION

### A. Mixed state case

In the main text, we consider a two-sided Lindblad equation for initially pure states. We consider a two-sided Lindblad equation for an initially mixed state case.

Let  $\rho_S$  be the initial mixed state in  $S$ . We consider an ancilla  $A$  that purifies  $\rho_S$ . Let  $|\tilde{\psi}_{SA}\rangle$  in  $S + A$  be a purification of  $\rho_S$ :

$$\rho_S = \text{Tr}_A \left[ |\tilde{\psi}_{SA}\rangle \langle \tilde{\psi}_{SA}| \right]. \quad (\text{S1})$$

We want to define the time evolution on a pure state in  $S + A$ . We introduce the following Kraus operators that act on  $S + A$ :

$$\tilde{V}_m \equiv V_m \otimes \mathbb{I}_A \quad (0 \leq m \leq M), \quad (\text{S2})$$

where  $V_m$  is defined in Eqs. (8) and (9). When we apply  $\tilde{V}_m$  to the purified state  $|\tilde{\psi}_{SA}\rangle$  and trace out the ancilla  $A$ , we obtain

$$\begin{aligned} \text{Tr}_A \left[ \sum_{m=0}^M \tilde{V}_m |\tilde{\psi}_{SA}\rangle \langle \tilde{\psi}_{SA}| \tilde{V}_m^\dagger \right] &= \text{Tr}_A \left[ \sum_{m=0}^M (V_m \otimes \mathbb{I}_A) |\tilde{\psi}_{SA}\rangle \langle \tilde{\psi}_{SA}| (V_m^\dagger \otimes \mathbb{I}_A) \right] \\ &= \sum_{m=0}^M V_m \text{Tr}_A \left[ |\tilde{\psi}_{SA}\rangle \langle \tilde{\psi}_{SA}| \right] V_m^\dagger \\ &= \sum_{m=0}^M V_m \rho_S V_m^\dagger, \end{aligned} \quad (\text{S3})$$

which shows that  $\tilde{V}_m$  induces the consistent time evolution for  $\rho_S$  in  $S$ . Using  $\tilde{V}_m$  defined in Eq. (S2), a pure state in  $S + A + E$  at  $t = \tau$  is represented by

$$|\tilde{\Psi}(\tau)\rangle = \sum_{\mathbf{m}} \tilde{V}_{m_{N-1}} \cdots \tilde{V}_{m_0} |\tilde{\psi}_{SA}\rangle \otimes |m_{N-1}, \dots, m_0\rangle, \quad (\text{S4})$$

As mentioned in the main text,  $\mathbf{m} = [m_{N-1}, \dots, m_1, m_0]$  is a measurement record when we observe the environment

---

\* [hasegawa@biom.t.u-tokyo.ac.jp](mailto:hasegawa@biom.t.u-tokyo.ac.jp)

$E$  with the projector  $\Pi(\mathbf{m}) = |\mathbf{m}\rangle \langle \mathbf{m}|$ . We calculate the probability of obtaining  $\mathbf{m}$ :

$$\begin{aligned}
P(m_{N-1}, \dots, m_0) &= \langle \tilde{\Psi}(\tau) | m_{N-1}, \dots, m_0 \rangle \langle m_{N-1}, \dots, m_0 | \tilde{\Psi}(\tau) \rangle \\
&= \langle \tilde{\Psi}(\tau) | \tilde{V}_{m_0}^\dagger \dots \tilde{V}_{m_{N-1}}^\dagger \tilde{V}_{m_{N-1}} \dots \tilde{V}_{m_0} | \tilde{\Psi}(\tau) \rangle \\
&= \text{Tr}_{SA} \left[ \tilde{V}_{m_{N-1}} \dots \tilde{V}_{m_0} | \tilde{\Psi}(\tau) \rangle \langle \tilde{\Psi}(\tau) | \tilde{V}_{m_0}^\dagger \dots \tilde{V}_{m_{N-1}}^\dagger \right] \\
&= \text{Tr}_S \left[ V_{m_{N-1}} \dots V_{m_0} \text{Tr}_A \left[ | \tilde{\Psi}(\tau) \rangle \langle \tilde{\Psi}(\tau) | \right] V_{m_0}^\dagger \dots V_{m_{N-1}}^\dagger \right] \\
&= \text{Tr}_S \left[ V_{m_{N-1}} \dots V_{m_0} \rho_S V_{m_0}^\dagger \dots V_{m_{N-1}}^\dagger \right].
\end{aligned} \tag{S5}$$

Therefore, statistics of  $\mathbf{m}$  obtained by quantum trajectories induced by  $V_m$  with an initially mixed state  $\rho_S$  is identical to the measurement on  $|\tilde{\Psi}(\tau)\rangle$  by  $\mathbb{I}_S \otimes \mathbb{I}_A \otimes \mathcal{G}$ .

In a similar manner, we introduce the Kraus operators  $\tilde{V}_{\star, m}$  that represent perturbed dynamics:

$$\tilde{V}_{\star, m} \equiv V_{\star, m} \otimes \mathbb{I}_A \quad (0 \leq m \leq M), \tag{S6}$$

where  $V_{\star, m}$  is defined in the main text. Similar to  $|\tilde{\Psi}(\tau)\rangle$ , the pure state of the conjugate dynamics in  $S + A + E$  at  $t = \tau$  is

$$|\tilde{\Psi}_\star(\tau)\rangle = \sum_{\mathbf{m}} \tilde{V}_{\star, m_{N-1}} \dots \tilde{V}_{\star, m_0} |\tilde{\psi}_{SA}\rangle \otimes |m_{N-1}, \dots, m_0\rangle. \tag{S7}$$

As in the main text, we can compute the fidelity

$$\begin{aligned}
\langle \tilde{\Psi}_\star(\tau) | \tilde{\Psi}(\tau) \rangle &= \text{Tr}_{SAE} \left[ | \tilde{\Psi}(\tau) \rangle \langle \tilde{\Psi}_\star(\tau) | \right] \\
&= \text{Tr}_{SA} \left[ \sum_{\mathbf{m}} \tilde{V}_{m_{N-1}} \dots \tilde{V}_{m_0} |\tilde{\psi}_{SA}\rangle \langle \tilde{\psi}_{SA}| \tilde{V}_{\star, m_0} \dots \tilde{V}_{\star, m_{N-1}} \right] \\
&= \text{Tr}_S \left[ \sum_{\mathbf{m}} V_{m_{N-1}} \dots V_{m_0} \rho_S V_{\star, m_0} \dots V_{\star, m_{N-1}} \right].
\end{aligned} \tag{S8}$$

The last line of Eq. (S8) yields a two-sided Lindblad equation with the initial state  $\rho$ .

## B. Measurement operator on the environment

The Kraus operator  $V_m$  in Eqs. (8) and (9) are not unique. Let  $\mathcal{B}$  be a unitary matrix. Any Kraus operator  $Y_m$  defined by

$$Y_n = \sum_m \mathcal{B}_{nm} V_m, \tag{S9}$$

yields the same time evolution as  $V_m$ , that is,  $\sum_m V_m \rho_S V_m^\dagger = \sum_m Y_m \rho_S Y_m^\dagger$ . A different Kraus operator corresponds to a different measurement on the environment  $E$ . The basis of the  $k$ th environmental subspace is  $|m_k\rangle$  where  $m_k \in \{0, 1, \dots, M\}$ , and, in this section, we simply write  $|m\rangle$  to express the subspace  $|m_k\rangle$ . The Kraus operator of Eqs. (8) and (9) corresponds to the measurement with basis  $|m\rangle$  for each subspace of the environment. Let us consider a different basis  $|\alpha\rangle$  representing a basis different from  $|m\rangle$ .  $|\alpha\rangle$  is related to  $|m\rangle$  via

$$|\alpha\rangle = \sum_m \mathcal{A}_{m\alpha} |m\rangle, \tag{S10}$$

where  $\mathcal{A}$  is a unitary operator. A direct calculation shows that the unitary operator  $\mathcal{A}$  satisfies  $\mathcal{A} = \mathcal{B}^\dagger$ , indicating that the unitary freedom in the Kraus operator corresponds to that in the measurement basis. By using  $|\alpha\rangle$  and  $Y_n$ , Eq. (10) can be represented by

$$|\Psi(\tau)\rangle = \sum_{\alpha} Y_{\alpha_{N-1}} \dots Y_{\alpha_0} |\psi_S\rangle \otimes |\alpha_{N-1}, \dots, \alpha_0\rangle, \tag{S11}$$



where  $\alpha \equiv [\alpha_{N-1}, \dots, \alpha_1, \alpha_0]$ . In the main text, we consider the counting observable defined in Eq. (11). In the main text, we consider a measurement on the environment by the projector  $\Pi(\mathbf{m}) = |\mathbf{m}\rangle\langle\mathbf{m}|$ . In this case, we observe a realization of  $\mathbf{m}$  and the principal system becomes an unnormalized state  $V_{m_{N-1}} \cdots V_{m_0} |\psi\rangle$ . Similarly, we can employ a different projector  $\tilde{\Pi}(\alpha) \equiv |\alpha\rangle\langle\alpha|$  for the environmental measurement. When using  $\tilde{\Pi}(\alpha)$ , we obtain a realization of  $\alpha$  and the principal system becomes an unnormalized state  $Y_{\alpha_{N-1}} \cdots Y_{\alpha_0} |\psi\rangle$ . Using  $\tilde{\Pi}(\alpha)$ , we can consider an Hermitian observable on the environment, which is expressed by

$$\tilde{\mathcal{G}} = \sum_{\alpha} \tilde{g}(\alpha) \tilde{\Pi}(\alpha), \quad (\text{S12})$$

where  $\tilde{g}(\alpha)$  is any function of  $\alpha$ . Because  $\langle\Psi_\star|\Psi\rangle$  does not depend on the environmental basis, Eq. (6) should hold for  $\tilde{\mathcal{G}}$  as well:

$$\left( \frac{[\tilde{\mathcal{G}}] + [\tilde{\mathcal{G}}]_\star}{\langle\tilde{\mathcal{G}}\rangle - \langle\tilde{\mathcal{G}}\rangle_\star} \right)^2 \geq \frac{1}{|\text{Tr}_S [e^{\mathcal{K}\tau} \rho_S(0)]|^{-2} - 1}. \quad (\text{S13})$$

$|\alpha\rangle$  can be arbitrary orthonormal basis in the environment, indicating that the main result of Eq. (6) holds for any continuous measurement.

In the main text, we consider a specific case that  $H_{S,\star} = 0$  and  $L_{\star,m} = 0$  for all  $m$ . In this case, the composite state of the conjugate dynamics at  $t = \tau$  is  $|\Psi_\star(\tau)\rangle = |\psi_S\rangle \otimes |0_{N-1}, \dots, 0_0\rangle$ , which is unchanged from the initial state. The counting observable  $\mathcal{G}$  of Eq. (11) satisfies

$$\langle\mathcal{G}\rangle_\star = \langle\Psi_\star(\tau)|\mathbb{I}_S \otimes \mathcal{G}|\Psi_\star(\tau)\rangle = 0, \quad (\text{S14})$$

$$\langle\mathcal{G}^2\rangle_\star = \langle\Psi_\star(\tau)|\mathbb{I}_S \otimes \mathcal{G}^2|\Psi_\star(\tau)\rangle = 0, \quad (\text{S15})$$

which leads Eq. (6) to Eq. (14). However, for  $\tilde{\mathcal{G}}$  defined in Eq. (S12), we generally have

$$\langle\tilde{\mathcal{G}}\rangle_\star = \langle\Psi_\star(\tau)|\mathbb{I}_S \otimes \tilde{\mathcal{G}}|\Psi_\star(\tau)\rangle \neq 0, \quad (\text{S16})$$

$$\langle\tilde{\mathcal{G}}^2\rangle_\star = \langle\Psi_\star(\tau)|\mathbb{I}_S \otimes \tilde{\mathcal{G}}^2|\Psi_\star(\tau)\rangle \neq 0. \quad (\text{S17})$$

Equations (S16) and (S17) shows

$$\frac{[\tilde{\mathcal{G}}]^2}{\langle\tilde{\mathcal{G}}\rangle^2} \not\geq \frac{1}{|\text{Tr}_S [e^{(-iH - \frac{1}{2} \sum_m L_m^\dagger L_m)\tau} \rho_S(0)]|^{-2} - 1}. \quad (\text{S18})$$

Therefore, Eq. (14) depends on how we perform the continuous measurement.

### C. Numerical simulation

In numerical simulation, we employ photon counting in a two-level atom driven by a laser field. As mentioned in the main text, the Lindblad equation of the system is specified by

$$H_S = \Delta |\epsilon_e\rangle\langle\epsilon_e| + \frac{\Omega}{2} (|\epsilon_e\rangle\langle\epsilon_g| + |\epsilon_g\rangle\langle\epsilon_e|), \quad (\text{S19})$$

$$L = \sqrt{\kappa} |\epsilon_g\rangle\langle\epsilon_e|, \quad (\text{S20})$$

where  $|\epsilon_g\rangle$  and  $|\epsilon_e\rangle$  denote ground and excite states, respectively;  $\Delta$ ,  $\Omega$ , and  $\kappa$  are model parameters. Kraus operators [Eqs. (8) and (9)] are

$$V_0 = \mathbb{I}_S - i\Delta t H_S - \frac{1}{2} \Delta t L^\dagger L, \quad (\text{S21})$$

$$V_1 = \sqrt{\Delta t} L. \quad (\text{S22})$$

where  $V_0$  and  $V_1$  correspond to no detection and detection of a jump event within  $\Delta t$ , respectively. Quantum trajectories generated by Eqs. (S21) and (S22) can be described by the following stochastic Schrödinger equation:

$$d\rho_S = -i[H_S, \rho_S]dt + \rho_S \text{Tr}_S [L \rho_S L^\dagger] - \frac{\{L^\dagger L, \rho_S\}}{2} dt + \left( \frac{L \rho_S L^\dagger}{\text{Tr}_S [L \rho_S L^\dagger]} - \rho_S \right) d\mathcal{N}. \quad (\text{S23})$$

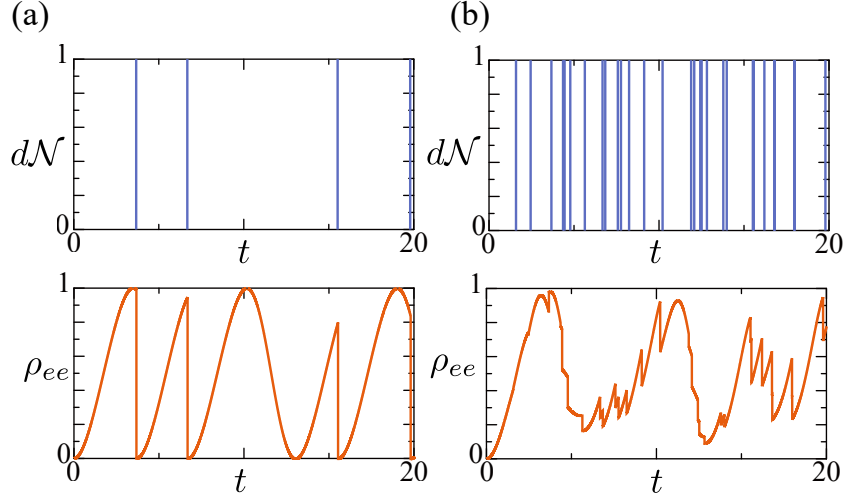


FIG. S1. Quantum trajectories generated by different measurement bases for a two-level atom driven by laser field (see Section S1 C for details). Trajectories are generated by (a)  $\zeta = 0$  and (b)  $\zeta = 1$ . Upper panels describe detection of jump events, and the lower panels show  $\rho_{ee} \equiv \langle \epsilon_e | \rho_S | \epsilon_e \rangle$  as a function of  $t$ .

When using Eqs. (S21) and (S22), numerical results are shown in Fig. 2(b) in the main text.

As shown in Eq. (S13), the main result [Eq. (6)] holds for arbitrary measurements on  $E$ . It is known, the Lindblad equation is invariant under the following transformation:

$$H_S \rightarrow H_S - \frac{i}{2}(\zeta^* L - \zeta L^\dagger), \quad (\text{S24})$$

$$L \rightarrow L + \zeta \mathbb{I}_S, \quad (\text{S25})$$

where  $\zeta \in \mathbb{C}$  can be arbitrary value. The corresponding Kraus operator is

$$Y_0 = \mathbb{I}_S - i\Delta t \left[ H_S - \frac{i}{2}(\zeta^* L - \zeta L^\dagger) \right] - \frac{1}{2}\Delta t (L^\dagger + \zeta^*)(L + \zeta), \quad (\text{S26})$$

$$Y_1 = \sqrt{\Delta t} (L + \zeta \mathbb{I}_S), \quad (\text{S27})$$

where  $Y_0$  and  $Y_1$  correspond to no detection and detection of a jump event, respectively.  $Y_0$  and  $Y_1$  [Eqs. (S26) and (S27)] and  $V_0$  and  $V_1$  [Eqs. (S21) and (S22)] are related via a unitary transformation shown in Eq. (S9), where  $\mathcal{B}$  is

$$\mathcal{B} = \begin{bmatrix} -\frac{1}{2}|\zeta|^2\Delta t + 1 & -\sqrt{\Delta t}\zeta^* \\ \sqrt{\Delta t}\zeta & -\frac{1}{2}|\zeta|^2\Delta t + 1 \end{bmatrix}. \quad (\text{S28})$$

We have shown that the measurement basis is transformed via Eq. (S10), where  $\mathcal{A} = \mathcal{B}^\dagger$ . Because Eq. (S28) shows that we can specify  $\mathcal{B}$  via  $\zeta$  alone, we can change the measurement basis by changing  $\zeta$ . Figure S1 shows trajectories generated by (a)  $\zeta = 0$  and (b)  $\zeta = 1$ . As explained above, trajectories of (a) and (b) use different measurement bases. Although the trajectories of (a) and (b) in Fig. S1 are very different, both cases reduce to the same dynamics on average.

In Eq. (S13), we have shown that the main result [Eq. (6)] holds for any measurement basis applied to  $E$  (that is, any unraveling of the Lindblad equation). We numerically verify that the main result [Eq. (6)] is satisfied for any measurement basis. To change the basis, we first randomly determine  $\zeta$ . For each dynamics (the original and the perturbed dynamics), we randomly select the model parameters  $\Delta$ ,  $\Omega$ , and  $\kappa$ . The time duration  $\tau$  and the initial density operator  $\rho_S$  is selected randomly as well. For the selected parameters and the density operator, we generate many quantum trajectories and calculate  $(\langle \mathcal{G} \rangle + \langle \mathcal{G} \rangle_\star)^2 / (\langle \mathcal{G} \rangle - \langle \mathcal{G} \rangle_\star)^2$ . In Fig. S2, we plot  $(\langle \mathcal{G} \rangle + \langle \mathcal{G} \rangle_\star)^2 / (\langle \mathcal{G} \rangle - \langle \mathcal{G} \rangle_\star)^2$  as a function of  $(\eta^{-1} - 1)^{-1}$  with  $\eta = |\text{Tr}_S[e^{\mathcal{K}\tau}\rho_S(0)]|^2$  by circles, where the dashed line denotes the lower bound. All circles are above the line, verifying Eq. (6) for different measurement bases.

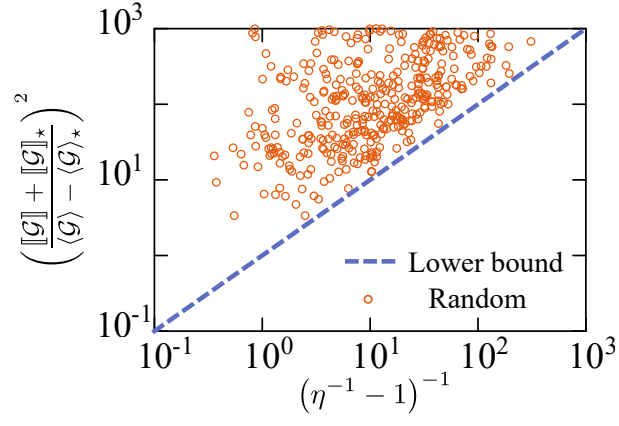


FIG. S2. Continuous measurement of the two-state atom for different measurement basis. Precision  $(\llbracket \mathcal{G} \rrbracket + \llbracket \mathcal{G} \rrbracket_*)^2 / ((\langle \mathcal{G} \rangle - \langle \mathcal{G} \rangle_*)^2)$  as a function of  $(\eta^{-1} - 1)^{-1}$ , where  $\eta = |\text{Tr}_S[e^{\mathcal{K}\tau} \rho_S(0)]|^2$ , for random realizations are plotted by circles. The dashed line denote the lower bound of the precision shown in Eq. (6). The parameter ranges are  $\Delta \in [0.1, 3.0]$ ,  $\Omega \in [0.1, 3.0]$ , and  $\kappa \in [0.1, 3.0]$  for each dynamics, and  $\tau \in [0.1, 1.0]$  and  $|\zeta| \in [0.0, 1.0]$ .